

Collective excitation spectrum of a disordered Hubbard model

Yolande H. Szczech, Michael A. Tusch and David E. Logan

University of Oxford, Physical and Theoretical Chemistry Laboratory, South Parks Road, Oxford

OX1 3QZ (U. K.)

Abstract

We study the collective excitation spectrum of a $d = 3$ site-disordered Anderson-Hubbard model at half-filling, via a random phase approximation (RPA) about broken-symmetry, inhomogeneous unrestricted Hartree-Fock (UHF) ground states. We focus in particular on the density and character of low-frequency collective excitations in the transverse spin channel. In the absence of disorder, these are found to be spin wave-like for all but very weak interaction strengths, extending down to zero frequency and separated from a Stoner-like band, to which there is a gap. With disorder present, a prominent spin wave-like band is found to persist over a wide region of the disorder-interaction phase plane in which the mean-field ground state is a disordered antiferromagnet, despite the closure of the UHF single-particle gap. Site-resolution of the RPA excitations leads to a microscopic rationalization of the evolution of the spectrum with disorder and interaction strength, and enables the observed localization properties to be interpreted in terms of the fraction of strong local moments and their site-differential distribution.

I. INTRODUCTION

Central to the understanding of any system with long-ranged order is a description of its collective excitations. If the Hamiltonian has a continuous symmetry which is broken in the ground state, their spectrum is gapless (as implied by the existence of Goldstone modes) and they dominate low-temperature thermodynamic properties.

One of the most familiar examples of such a system is the Heisenberg model, whose collective excitations are pure spin waves. With $S = \frac{1}{2}$, antiferromagnetic (AF) nearest-neighbour interactions and on a bipartite lattice, the ground state of the Hamiltonian has long-ranged magnetic order in three dimensions d^1 . While no exact solution exists for $d > 1$, a successful and longstanding approach to the ground state and collective excitations of the model is given by linear spin-wave theory (LSW)², in which particle-hole pairs created out of the Néel mean-field ground state are treated as bosons. The theory becomes exact in the limit $d \rightarrow \infty$, and $1/d$ corrections can be systematically incorporated^{3,4}; but even in $d = 2$, LSW estimates for the sublattice magnetization, spin wave velocity and ground state energy are in good agreement with quantum Monte Carlo calculations (QMC) (see e.g. Ref. 3 for a comprehensive review).

It is well known that the AF Heisenberg model represents the strong coupling limit of the half-filled Hubbard model⁵. At finite interaction strengths U , the mean-field ground state remains the Néel state (albeit with self-consistently determined local moment magnitudes) and gives a qualitatively sound description of the true ground state in $d \geq 2$. The collective excitation spectrum is however considerably more complex than that of the Heisenberg model, since its low-frequency spin wave excitations are mixed with incoherent, Stoner-like processes, leading to $O(N^2)$ particle-hole excitations in contrast to the N spin waves which alone survive in the strong-coupling limit.

The generalization of LSW to finite interaction strengths is given by the random phase approximation (RPA) about the fully unrestricted Hartree-Fock (UHF) saddle point. Although naively thought of as a weak-coupling theory, it reduces precisely to LSW in the

strong coupling limit, an observation which has led a number of authors to conclude it to be a sound way of probing the collective excitations of the Hubbard model over a wide range of interaction strengths: for example, such an approach has been successfully used to investigate the transverse spin excitation spectrum of the Hubbard model both in $d = 1$ ⁶ and $d = 2$ (see e.g. Refs 7, 8, 9).

In the present work we consider initially the collective excitation spectrum of the Hubbard model on a simple cubic lattice. This is shown to possess two distinct bands for all interaction strengths U : a low-energy spin wave-like band corresponding primarily to orientational fluctuations of the local moments, extending down to zero frequency and containing two Goldstone modes; and an upper band of Stoner-like excitations, to which there is a gap due to Fermi-surface nesting in the corresponding single-particle spectrum¹⁰. The latter involve a significant degree of charge transfer character (site double-occupancy) and are projected out in the large U limit, leaving solely the low-frequency excitations, which become the pure spin waves of the Heisenberg model. It is found that, despite mixing between the two bands at finite U , the low-frequency excitations retain a strong degree of spin wave character down to weak interaction strengths.

A problem about which very little is known, even at a qualitative level, is the effect of disorder on the collective excitation spectrum. In a disordered system, the collective excitations are governed by the interplay of a number of complex processes, including strong correlations of particle-hole pairs, Anderson localization of the underlying single-particle states, and the non-trivial statistics associated with the distributions of local charges and magnetic moments arising from inhomogeneity in the site environments.

Even at the mean field level of UHF, the combined effects of disorder and electron interactions in leading to strongly inhomogeneous ground states yield rich behaviour, as shown by a recent study of the zero-temperature UHF phase diagram of a site-disordered Anderson-Hubbard model¹¹ (AHM). Further, at RPA level, these ground states in turn give rise to strongly inhomogeneous magnetic response properties^{12,13}. In particular, disorder is found to lead to a significant enhancement in local static susceptibilities over those in the

pure system, this enhancement being strongly site-differential.

The behaviour of static and dynamic susceptibilities in both the spin and charge channels ultimately reflects the character and distribution of collective excitations about the ground state. The observed site-differential enhancements mentioned above naturally raise questions both of how disorder affects the excitation spectra of the model and of the spatial distribution and localization characteristics of the excitations. In addition, the stability of the long-ranged order present in the mean-field ground state towards zero point spin fluctuations, and the low-temperature properties of the model, are also governed by the RPA excitations.

We here investigate of the RPA spectrum of a $d = 3$ Anderson-Hubbard model with Gaussian site-disorder, throughout the disorder-interaction phase plane. In Section II, we discuss generic properties of the model and describe the procedure for calculating and characterizing the collective excitation spectrum at RPA level. After a brief discussion of the pure Hubbard model in Section III, we focus in Section IV on the AHM, concentrating on the distribution, character and localization properties of the low-frequency excitations, with particular emphasis on the existence or otherwise of a spin wave-like band in the transverse excitation spectrum at finite disorder. We conclude in Section V with a discussion of the extent to which a recently developed mapping of the excitations of the Hubbard model^{14,15} onto those of an effective spin model, can be applied to the disordered system.

II. COLLECTIVE EXCITATION SPECTRUM AT RPA LEVEL

The Hamiltonian we consider is given by

$$H = \sum_{i,\sigma} \epsilon_i n_{i\sigma} - t \sum_{\langle ij \rangle, \sigma} c_{i\sigma}^\dagger c_{j\sigma} + \frac{1}{2} U \sum_{i,\sigma} n_{i\sigma} n_{i-\sigma} \quad (2.1)$$

where t is the hopping matrix element, U is the (repulsive) on-site Coulomb interaction and the $\langle ij \rangle$ sum is over nearest neighbour sites on a $d = 3$ simple cubic lattice. The site energies $\{\epsilon_i\}$ are drawn randomly from a common Gaussian distribution $g(\epsilon)$ of variance Δ^2 which, together with Eq. (2.1), specifies the Anderson-Hubbard model considered here; and we

focus exclusively on half-filling. Making a spin-rotationally invariant UHF approximation to the interaction term in Eq. (2.1) allows the Hamiltonian to be expressed as $H = H_0 + H_1$ with

$$H_0 = \sum_{i,\sigma} \epsilon_i n_{i\sigma} - t \sum_{\langle ij \rangle, \sigma} c_{i\sigma}^\dagger c_{j\sigma} + U \sum_i \left\{ \frac{1}{2} \bar{n}_i n_i - 2 \bar{\mathbf{S}}_i \cdot \mathbf{S}_i \right\} , \quad (2.2)$$

where \mathbf{S}_i is a spin- $\frac{1}{2}$ operator and the overbar denotes an expectation over the UHF ground state. The zero-temperature phase diagram of H_0 in the $(\Delta/t, U/t)$ plane has been discussed extensively in Ref. 11; aspects of this study necessary for the present work will be summarized briefly in §IVA. Here we note that, while a rich variety of phases arises, all mean-field magnetic ground states are found to be Ising-like (i.e. fully collinear local moments, with $\bar{S}_{ix} = 0 = \bar{S}_{iy}$ for all sites i), with $S_z^{\text{tot}} = \sum_i \bar{S}_{iz} = 0$. Collective excitations about these ground states, obtained via the RPA, then decouple into two sets¹²: for frequencies $\omega \geq 0$ there exist $N^2/2$ spin excitations transverse to the local moment z -axis, and $N^2/2$ longitudinal spin and charge excitations. In the non-disordered ($\Delta/t = 0$) Hubbard model there is a gap to longitudinal spin excitations for all U/t ¹², reflecting the presence of a gap in the single-particle density of states (DoS). By contrast the transverse excitation spectrum is gapless (as reflected by the presence of Goldstone modes). With disorder present, the dominant low-energy collective excitations are again found in the transverse spin channel. We thus focus here on the transverse spin spectrum, since it is these excitations which govern measured susceptibilities (the existence of a spin-flop transition implying that only transverse excitations are in practice probed¹³), and which are dominant in determining low-temperature thermodynamic properties.

A. Determination of the transverse excitation spectrum

The equations of motion for the RPA particle-hole excitations are straightforwardly derived (see e.g. Ref. 16). However, solution of these equations requires diagonalization of a

$2N^2 \times 2N^2$ non-Hermitian matrix, a procedure limited to impractically small system sizes. An alternative —and viable— procedure is to exploit the fact that, because the interaction term H_1 contains only on-site terms, expressions for the RPA dynamic susceptibilities (derived either diagrammatically or via linear response theory¹²), involve only matrices of order N . Specifically, the transverse spin susceptibility

$$\chi_{ij}^{-+}(\omega) = i \int dt e^{i\omega t} \langle 0 | \mathcal{T} \{ S_i^-(t) S_j^+ \} | 0 \rangle_{\text{RPA}} , \quad (2.3)$$

is given by

$$\chi^{-+}(\omega) = {}^0\chi^{-+}(\omega) \left[\mathbf{1} - U {}^0\chi^{-+}(\omega) \right]^{-1} , \quad (2.4)$$

where the $N \times N$ matrix ${}^0\chi^{-+}(\omega)$ is the corresponding UHF transverse susceptibility obtained by replacing $|0\rangle_{\text{RPA}}$ by $|0\rangle_{\text{UHF}}$ in Eq. (2.3). This is in turn given explicitly by

$$\begin{aligned} {}^0\chi_{ij}^{-+}(\omega) = \sum_{\alpha > F > \beta} \left\{ \frac{a_{i\alpha\uparrow} a_{j\alpha\uparrow} a_{i\beta\downarrow} a_{j\beta\downarrow}}{E_{\alpha\uparrow} - E_{\beta\downarrow} - \omega - i\eta} \right. \\ \left. + \frac{a_{i\alpha\downarrow} a_{j\alpha\downarrow} a_{i\beta\uparrow} a_{j\beta\uparrow}}{E_{\alpha\downarrow} - E_{\beta\uparrow} + \omega - i\eta} \right\}. \end{aligned} \quad (2.5)$$

Here F is the Fermi level, $\eta = 0+$ and the $\{E_{\alpha\sigma}\}$ are the UHF single-particle energies, with eigenvectors $|\Psi_{\alpha\sigma}\rangle = \sum_i a_{i\alpha\sigma} |\phi_{i\sigma}\rangle$ expanded in a site basis (and which are pure spin-orbitals for Ising-like UHF solutions¹¹). We add in passing that the Fermi energy is pinned at $E_F = \frac{1}{2}U$ for all disorder strengths $\Delta \geq 0$, since the familiar particle-hole symmetry characteristic of the non-disordered limit is preserved for all $\Delta > 0$ with the symmetric Gaussian $g(\epsilon)$ ¹¹.

Eq. (2.5) is just the Lehmann representation for the retarded polarization propagator appropriate to the UHF ground state, with poles at the Stoner excitation energies. When ω does not coincide with a pole, this real symmetric matrix is diagonalized by an orthogonal matrix $\mathbf{V}(\omega)$ with eigenvalues $\{\lambda_\gamma(\omega)\}$. Most importantly, as is evident from Eq. (2.4), this transformation also diagonalizes $\chi^{-+}(\omega)$ with corresponding eigenvalues $\lambda_\gamma(\omega)/[1 - U\lambda_\gamma(\omega)]$, viz:

$$\chi_{ij}^{-+}(\omega) = \sum_{\gamma} V_{i\gamma} \frac{\lambda_{\gamma}(\omega)}{1 - U\lambda_{\gamma}(\omega)} V_{j\gamma} \quad (2.6)$$

RPA transverse collective excitations correspond to the ω -poles of $\chi^{-+}(\omega)$, which thus occur at $1 - U\lambda_{\gamma}(\omega) = 0$, i.e. whenever an eigenvalue of ${}^0\chi^{-+}(\omega)$ crosses $1/U$. Further, since $\chi_{ij}^{+-}(\omega) = \chi_{ji}^{-+}(-\omega)$, a knowledge of the (positive and negative) poles of $\chi^{-+}(\omega)$ alone is sufficient to determine the full transverse spin excitation spectrum.

Two final points concerning the poles $\chi^{-+}(\omega)$ should be made before proceeding. First, the broken symmetry of any magnetic UHF state implies the presence of a zero-frequency Goldstone mode in both χ^{-+} and χ^{+-} , ensuring that the transverse excitation spectrum is gapless. Second, the ω -poles occur correctly on the real axis only if the UHF ground state is fully stable against particle-hole excitations (see e.g. Ref. 17). An eigenstate of H_0 which is not a true minimum on the UHF total energy surface leads to imaginary- ω excitations which carry the system away from the saddle point, rendering it unstable. In this regard, and even when the mean-field *solutions* are Ising-like, use of a fully unrestricted and spin-rotationally invariant Hartree-Fock approximation is an essential prerequisite, since it ensures the mean-field states are minima.

In studying collective excitations at RPA level, a pole search on $\chi^{-+}(\omega)$ (Eqs (2.4,5)) is powerful, since it allows study of much larger system sizes than direct solution of the RPA equations. We now outline this procedure. From Eq. (2.5), ${}^0\chi^{-+}(\omega)$ itself has poles at the UHF excitation energies but, in the intervals between the poles, the eigenvalues $\{\lambda_{\gamma}(\omega)\}$ of ${}^0\chi^{-+}(\omega)$ are continuous functions of ω . For a given disorder realization, we thus determine the excitation spectrum as follows. (i) Solution of the UHF problem yields the UHF excitation energies and hence the intervals over which the eigenvalues $\lambda_{\gamma}(\omega)$ are finite. (ii) Diagonalization of ${}^0\chi^{-+}(\omega)$ for ω at the beginning and the end of each interval yields the number of eigenvalues which have crossed $1/U$ —and hence the number of RPA poles—in each interval. (iii) Finer resolution may then be obtained using, for example, a bisection technique.

B. Character of the transverse excitations

Important information concerning the character of a given excitation of frequency ω_p can be obtained from the eigenvector coefficients $\{V_{i\gamma}(\omega_p)\}$.

In the strong coupling limit $U/t \rightarrow \infty$, the resultant AF Heisenberg model contains N transverse particle-hole excitations, corresponding to linear combinations of solely on-site spin flips. These are just the familiar pure spin waves. At finite U/t , off-site spin flip excitations also contribute to the transverse spectrum, such that while there is spin-charge separation (in the sense that the transverse spin and longitudinal/charge channels decouple¹²), the transverse excitations themselves possess some charge-transfer character. It is particularly instructive to evaluate the on-site spin flip (or spin wave) contribution to a given excitation, as now considered.

The Lehmann representation for the diagonal elements of the RPA susceptibility is given generally by

$$\chi_{ii}^{-+}(\omega) = \sum_n \frac{|\langle 0|S_i^-|n\rangle|^2}{\mathcal{E}_{n0} - \omega - i\eta} + \frac{|\langle 0|S_i^+|n\rangle|^2}{\mathcal{E}_{n0} + \omega - i\eta} \quad (2.7)$$

where $|0\rangle$ and $|n\rangle$ are RPA ground and excited states and \mathcal{E}_{n0} are the RPA excitation energies. From Eq. (2.6), $\chi_{ii}^{-+}(\omega)$ is expressible in terms of the eigenvalues and eigenvectors of ${}^0\chi^{-+}(\omega)$:

$$\chi_{ii}^{-+}(\omega) = \sum_{\alpha} V_{i\alpha}^2(\omega) \frac{\lambda_{\alpha}(\omega)}{1 - U\lambda_{\alpha}(\omega)} \quad (2.8)$$

To compare Eqs (2.7) and (2.8), we analytically continue Eq. (2.8) by the replacement $\lambda_{\alpha}(\omega) \rightarrow \lambda_{\alpha}(\omega + is)$, where s is an infinitesimal. Consider any particular pole, ω_p , of Eq. (2.8), such that $\lambda_{\gamma}(\omega_p) = 1/U$. For frequencies $\omega \simeq \omega_p$, $\chi_{ii}^{-+}(\omega)$ is dominated by the $\alpha = \gamma$ term and is given to leading order by

$$\chi_{ii}^{-+}(\omega \simeq \omega_p) = \frac{V_{i\gamma}^2(\omega_p)}{U^2 \left(\frac{\partial \lambda_{\gamma}}{\partial \omega} \right)_{\omega_p} (\omega_p - \omega - is)} \quad (2.9)$$

Comparison of Eqs (2.9) and (2.7) implies

$$\text{sgn}\left(\frac{\partial\lambda_\gamma}{\partial\omega}\right)_{\omega_p} = \text{sgn}(\omega_p) \quad , \quad (2.10a)$$

and

$$\text{sgn}(s) = \text{sgn}(\omega_p) \quad (2.10b)$$

(in order that the poles of $\chi^{-+}(\omega)$ occur in the correct half-plane); together with the central result that, for the given pole,

$$|\langle 0|S_i^\rho|n\rangle|^2 = \frac{1}{U^2 \left| \frac{\partial\lambda_\gamma}{\partial\omega} \right|_{\omega_p}} V_{i\gamma}^2(\omega_p) \quad (2.11)$$

where $\rho = -\text{sgn}(\omega_p)$. Further, since the eigenvector coefficients $\{V_{i\gamma}(\omega)\}$ are by construct normalized, the sum rule

$$\sum_i |\langle 0|S_i^\rho|n\rangle|^2 = \frac{1}{U^2 \left| \frac{\partial\lambda_\gamma}{\partial\omega} \right|_{\omega_p}} \quad (2.12)$$

follows. That this sum is not unity simply reflects the fact that, at finite U/t , RPA transverse spin excitations have finite weight outside the on-site spin flip subspace, i.e. matrix elements of the form $\langle 0|c_{i\downarrow}^\dagger c_{j\uparrow}|n\rangle$ with $i \neq j$ are non-zero; for example it may be shown that the general RPA normalization expressed in a site basis implies that $\sum_{ij} |\langle 0|c_{i\downarrow}^\dagger c_{j\uparrow}|n\rangle|^2 = 1$ for RPA excitations corresponding to positive- ω poles. Only in the strong coupling limit $U/t \rightarrow \infty$ are these off-site excitations effectively projected out of the transverse spin spectrum.

The interpretation of the eigenvectors $\{\mathbf{V}_\gamma(\omega)\}$ is therefore clear: from Eqs (2.11) and (2.12) the set of coefficients $\{V_{i\gamma}(\omega_p)\}$ corresponding to a particular $\lambda_\gamma(\omega_p) = \frac{1}{U}$ describe the spatial distribution of the on-site spin flip component of the collective excitation, while the prefactor $\Omega(\omega_p) = 1/(U^2 |\partial\lambda_\gamma/\partial\omega|_{\omega_p})$ gives the weight of the RPA excitation in the subspace of on-site spin flips. Excitations with $\Omega(\omega_p) \simeq 1$ are predominantly spin waves, while those with $\Omega(\omega_p) \ll 1$ have significant off-site ‘charge transfer’ character. (Note that, to generalize to a disordered system, we use the term ‘spin wave’ to denote any excitation with $\Omega \simeq 1$, regardless of its \mathbf{q} -resolution.)

The above interpretation may also be exploited to define an inverse participation ratio (IPR) for the collective excitations, in analogy to the familiar IPR employed in the study of localization of single-particle states¹⁸, via

$$L(\omega_p) = \sum_i V_{i\gamma}^4(\omega_p) \quad . \quad (2.13)$$

Using Eq. (2.12), this may be expressed as

$$L(\omega_p) = \frac{\sum_i |\langle 0 | S_i^\rho | n \rangle|^4}{(\sum_i |\langle 0 | S_i^\rho | n \rangle|^2)^2} \quad : \rho = -\text{sgn}(\omega_p) \quad . \quad (2.14)$$

$L(\omega_p)$ is on the order of the inverse of the number of sites overlapped by the excitation at ω_p : for an excitation receiving uniform contributions from m sites, $L(\omega) \sim 1/m$. In the thermodynamic limit, $L(\omega)$ is thus zero for a delocalized excitation and non-zero for a localized excitation. For a finite-sized system $L > 0$ necessarily, requiring the estimation of a threshold IPR, appropriate to a given system size. While for the single-particle excitations of the (non-interacting) Anderson model, such a threshold IPR can be addressed via finite-size scaling¹⁹, we have no information on the N -scaling of $L(\omega)$ in the present system. In §IV, however, we argue that a qualitative understanding of the localization characteristics of transverse spin excitations may nonetheless be obtained.

III. EXCITATION SPECTRUM OF THE PURE HUBBARD MODEL

Before discussing the effects of disorder on the transverse excitation spectrum of the Anderson-Hubbard model, we first consider briefly the important non-disordered limit. In this case, for all $U/t > 0$, the UHF single-particle spectrum $D(E) = \frac{1}{2} \sum_{\alpha\sigma} \delta(E - E_{\alpha\sigma})$ has a band gap of magnitude $U|\mu|$, with $|\mu|$ the self-consistent UHF local moment magnitude; and in which lies the Fermi level $E_F = \frac{1}{2}U^{10}$. Consequently, the pure UHF particle-hole excitation spectrum consists of a single Stoner band beginning at $\omega = U|\mu|$, with a maximum at $\omega \sim U$. The full RPA spectrum of collective transverse spin excitations consists, by contrast, of two distinct components (we consider $\omega \geq 0$ throughout, since the spectrum is symmetric in ω).

First, a low frequency band containing precisely N excitations of predominantly spin wave character (discussed below), and extending down to $\omega = 0$ as implied by the presence of the Goldstone modes for all $U/t > 0$. Second, a high frequency band containing $(N/2)(N - 2)$ Stoner-like excitations, which closely resembles the corresponding pure UHF transverse spin spectrum: it begins at $\omega = U|\mu|$ —the gap in the UHF single-particle spectrum— and has maximum spectral density for $\omega \sim U$. This Stoner-like band is effectively eliminated as $U \rightarrow \infty$. For all $U/t > 0$, however, it may be shown to be separated from the top of the low frequency band by a spectral gap, i.e. there is a persistent separation of scales between the low energy spin wave-like band and higher energy Stoner-like excitations. For this reason we focus exclusively on the low- ω component of the spectrum.

The prescription of §II, reformulated in a two-sublattice basis⁷ appropriate to the half-filled, non-disordered model, allows the RPA spectrum to be determined; in practice we find that a lattice of 32^3 \mathbf{q} -points (corresponding to $N = 32768$) is required to give a sufficiently dense spectrum. Fig. 1 shows the resultant density of the lowest N transverse spin excitations, given by

$$N_T(\omega) = N^{-1} \sum_{\omega_p \leq \omega_{\max}} \delta(\omega - \omega_p) \quad (3.1)$$

where ω_{\max} is the frequency of the N^{th} excitation, for large coupling $U/t = 20$. Also shown is the corresponding spectrum for the AF Heisenberg model with solely nearest-neighbour (NN) $J = 4t^2/U$, given by $N_T^{\text{LSW}}(\omega) = N^{-1} \sum_{\mathbf{q}} \delta(\omega - \omega_{\mathbf{q}})$ with²

$$\omega_{\mathbf{q}} = \pm 3J \sqrt{1 - \gamma_{\mathbf{q}}^2} \quad (3.2)$$

where $\gamma_{\mathbf{q}} = \frac{1}{3} \sum_{\alpha=1}^3 \cos(q_{\alpha}a)$ and a is the lattice constant. The spectrum of low-frequency transverse spin excitations of the Hubbard model thus closely resembles that of the NN Heisenberg model at large U/t —as expected, since as $U/t \rightarrow \infty$ the former maps exactly onto the latter— although as seen there is a not inappreciable quantitative difference even for $U/t = 20$.

Less predictably, this qualitative similarity persists down to weak coupling. However, as U/t is decreased, the energy scale for low-frequency RPA excitations rapidly deviates from

that of the NN Heisenberg model with $J = 4t^2/U$. Fig. 2 shows the effects of gradually decreasing U/t down to $U/t = 2$. Initially, the spin-wave band is pushed to *higher* energy, consistent with the strengthening of NN exchange couplings and reflecting also the increasing importance of beyond-nearest neighbour couplings as shown in a recent paper¹⁴. Below $U/t \sim 5$, however, this band starts to migrate to *lower* energies, reflecting an increasing repulsion with the approaching Stoner-like band.

To investigate quantitatively the spin-wave character of the excitations, we calculate $\Omega(\omega_p) = 1/(U^2|\partial\lambda/\partial\omega|_{\omega_p})$ for $\omega_p \leq \omega_{\max}$. The lowest excitation is of course the Goldstone mode corresponding to a global spin rotation, and is a pure spin wave for all $U/t > 0$: $\Omega(\omega_p = 0) = 1$. Since excitations at the upper edge of the spin wave-like band are naturally most strongly influenced by the encroaching Stoner-like band, it is found that $\Omega(\omega_p) > \Omega(\omega_{\max})$ for all $\omega_p < \omega_{\max}$. The first column of Table I thus shows the U/t -dependence of $\Omega(\omega_{\max})$. From this it is seen that for $U/t \gtrsim 3$ the excitations are predominantly spin waves – in fact for $U/t \gtrsim 5$ they are in essence pure spin waves, $\Omega = 1$ —commensurate with a significant gap between the spin wave and Stoner-like bands. For $U/t \lesssim 2 - 3$, this gap diminishes rapidly and there is a substantial loss of spin wave character for excitations with $\omega \simeq \omega_{\max}$. Nonetheless, as is evident from the above, the low energy transverse spin excitations of the Hubbard model remain predominantly spin waves for all but the lowest U/t .

IV. ANDERSON-HUBBARD MODEL

Before considering the effects of disorder on the RPA spectrum, we first briefly outline relevant properties of the inhomogeneous UHF ground state, since it is particle-hole excitations out of this state which form the basis for the RPA collective modes; a full account of the mean-field phase diagram is given in Ref. 11.

A. Mean-field ground state

On the introduction of disorder, UHF solutions remain Ising-like, with $S_z^{\text{tot}} = 0$. Three distinct magnetic phases are found: disordered paramagnetic (P), antiferromagnetic (AF) and spin glass-like (SG) phases. Both metallic (M) and insulating (I) phases also occur, with the dominant metal-insulator transition (MIT) $M \rightarrow$ gapless I, driven by Anderson localization of single-particle states at the Fermi energy $E_F = \frac{1}{2}U$. We now consider two specific paths across the disorder-interaction phase plane, which will be employed in the next section to illustrate the combined effects of Δ and U on the RPA transverse spin spectrum.

First, consider fixing $U/t = 12$ and varying disorder, Δ/t . As Δ/t is increased from zero, disorder leads to broadening and eventual overlap of the Hubbard bands in the UHF single-particle spectrum, such that E_F lies within a pseudogap in the total DoS $D(E)$. Studies of the IPR $L'(E) = \sum_i |a_{i\alpha\sigma}|^4$ for single-particle states of energy $E_{\alpha\sigma} = E$, with $E \sim E_F$ ¹¹, imply that the system passes directly from a gapped to gapless insulator in this region of the $(\Delta/t, U/t)$ phase plane (at $\Delta/t \simeq 2.5$). Fig 3(A) shows $D(E)$ and the IPR profile $L'(E)$ averaged over $N = 512$ site disorder realizations for $(\Delta/t, U/t) = (3, 12)$. A pronounced pseudogap is evident in $D(E)$, in which E_F lies. Correspondingly, $L'(E)$ shows a maximum at $E = E_F$ and minima for states in the centre of the Hubbard bands where $D(E)$ is maximal. Using a threshold IPR appropriate to the chosen system size¹¹ shows that Fermi level states are localized: the system is a gapless Mott-Anderson insulator (and remains thus with increasing Δ/t at the chosen $U/t = 12$). Analysis of the Fourier transform of the local moment $S_z(\mathbf{k}) = N^{-1} \sum_i \mu_i e^{i\mathbf{k} \cdot \mathbf{R}_i}$ shows however that the system remains antiferromagnetically ordered: although increasingly ‘dirtied’ by disorder, $|S_z(\boldsymbol{\pi})| \simeq |\mu|$ (where the mean moment per site $|\mu| = N^{-1} \sum_i |\mu_i|$), with little weight at other \mathbf{k} -vectors. Note however that while the phases of the moments remain locked in AF alignment, the distribution of local moment *magnitudes* over the sites is highly disordered. This is evident from the site-resolved distribution of local moment magnitudes, $|\mu(\epsilon)| = N_\epsilon^{-1} \sum_{i:\epsilon_i=\epsilon} |\mu_i|$, with N_ϵ the number of sites with $\epsilon_i = \epsilon$; as shown in Fig 3(B), again for $(\Delta/t, U/t) = (3, 12)$.

Sites with energies $|\epsilon_i| \lesssim \frac{1}{2}U$, disposed randomly on the lattice, carry strong atomic-like moments, while sites with lower or higher site energies have $|\mu_i| \simeq 0$, being respectively largely doubly occupied by electrons or empty. This profile is found to vary little with disorder for fixed $U/t = 12$, aside from minor erosion of local moment magnitudes: the primary effect of Δ/t is to determine, via the site-energy distribution $g(\epsilon)$, the fraction of sites (around $\epsilon = 0$) which carry strong local moments.

Also shown in Fig. 3(B) is a measure of the distribution of quasiparticle states of *given* energy E over the sites: $H(\epsilon; E)$, given by¹¹

$$H(\epsilon; E) = \frac{g(\epsilon)D(\epsilon; E)}{D(E)}, \quad (4.1a)$$

where

$$D(\epsilon; E) = \frac{1}{2}N_\epsilon^{-1} \sum_{i:\epsilon_i=\epsilon} \sum_{\alpha\sigma} |a_{i\alpha\sigma}|^2 \delta(E - E_{\alpha\sigma}) \quad (4.1b)$$

is the partial density of states for sites of bare site energy ϵ . $H(\epsilon; E_F)$ is thus the quantum probability density that electrons in Fermi-level quasiparticle states will be found on sites of bare site energy ϵ . As discussed in Ref. 11, and exemplified in Fig. 3(B), $H(\epsilon; E_F)$ is peaked strongly at the boundaries of the local moment distribution $|\epsilon| \simeq \frac{1}{2}U$; i.e. sites with strong local moments participate but weakly in Fermi-level quasiparticle states, which are in contrast dominated by sites with bare site energies close to the local moment boundaries. Sites with strong local moments, around $\epsilon = 0$, are in turn found to contribute mainly to quasiparticle states with $E \simeq 0$ and $E \simeq U$, i.e. around the maxima in the single-particle spectrum.

The second path considered is fixing the disorder at $\Delta/t = 3$, and decreasing the scaled interaction strength U/t from $U/t = 12$. Note that, since the $U/t \rightarrow \infty$ limit of the disordered Hubbard model for any Δ/t is the *non-disordered* AF Heisenberg model, decreasing U/t may be thought of as effectively increasing (by ‘switching on’) the role of disorder. As U/t is reduced, the fraction of sites at the local moment boundaries $\sim g(\pm\frac{1}{2}U)$ —which give the dominant contribution to Fermi-level states (Fig. 3(B))— increases. The system

is ultimately driven metallic at a critical $U/t \simeq 7.2^{11}$. However, magnetic ordering remains characterized by a strong peak in $S_z(\mathbf{k})$ at $\mathbf{k} = \boldsymbol{\pi}$ until $U/t \simeq 2.5$, whereupon a sharp¹² transition occurs to a spin glass-like state, with $S_z(\mathbf{k})$ receiving essentially uniform $O(1/N)$ contributions from many \mathbf{k} vectors; see Ref. 12. In this phase, although the mean local moment per site $|\mu|$ is typically small (~ 0.05), relatively strong local moments are in fact found on a small fraction of sites with $|\epsilon| \lesssim \frac{1}{2}U$ for a given disorder realization. As discussed in Ref. 11, this reflects the disorder-induced production of statistically rare local environments in which atomic-like moments are not significantly eroded by electron hopping processes.

B. Collective excitation spectrum of the Anderson-Hubbard model

We now turn to the effects of disorder on the transverse RPA excitation spectrum. The principal questions we seek to address are:

- What is the effect of disorder on the density of transverse spin excitations? Does a low-energy spin wave-like band exist for finite disorder, and what is the character of the associated excitations?
- What is the effect of disorder on the localization characteristics of low-lying collective excitations?
- What is the distribution of transverse spin excitations of given energy over the sites, and how does this relate to the inhomogeneous distribution of local moments in the mean-field ground state?

With disorder present, there are no simplifying symmetries which allow very large system sizes to be studied, as in the $\Delta = 0$ case. However, this lack of symmetry —specifically, the absence of degeneracies in the UHF spectrum— enables reasonable statistics to be gained by sampling many disorder realizations for system sizes much smaller than those required for $\Delta = 0$. Numerical evaluation of the entire transverse excitation spectrum —including the Stoner-like excitations—remains nonetheless a large problem: a full pole search for a system

of N sites requires diagonalization of a $N \times N$ matrix in the vicinity of $\frac{1}{2}N^2$ poles, and is therefore $O(N^4)$ for each disorder realization; an ensemble of which needs subsequently to be sampled. For calculations of the full transverse spin spectrum we have thus chosen $N = 64$ site systems, which are found to be sufficient for reproduction of its general features; while for more detailed study of the low energy portion $N = 216$ is employed.

For fixed disorder $\Delta/t = 3$ and various values of the interaction strength $U/t \leq 12$, Fig. 4 shows the full RPA density of transverse spin excitations, together with the corresponding UHF particle-hole excitation spectrum (the ‘pure Stoner’ spectrum). At $U/t = 12$, where the mean-field ground state is a gapless AF insulator, a pronounced spin wave-like band is again evident in the RPA spectrum at low ω , as for the non-disordered limit (although the pure Stoner spectrum now extends down to $\omega = 0$); the remainder of the RPA spectrum closely resembles the Stoner spectrum. On decreasing U/t , the pure Stoner spectrum shifts to lower energy, since the separation between the maxima in the corresponding single-particle spectrum $D(E)$ decreases and the pseudogap at E_F is gradually eliminated. As a result, the spin wave-like band is gradually shifted to lower energy (‘softened’) by, and ultimately absorbed into, the Stoner-like band. By $U/t = 3$, close to the AF-SG border, the pure Stoner and RPA spectra appear virtually indistinguishable.

On fixing U/t and increasing disorder, a somewhat different picture emerges. Fig. 5 shows the RPA and pure Stoner spectra for $U/t = 12$ and various values of Δ/t . At low disorder $\Delta/t = 1$, for which the UHF ground state is a AF Mott-Hubbard (gapped) insulator, a spin wave-like band, well separated from the remainder of the excitations, is clearly distinguishable. Closer resolution shows that this band is in fact shifted to slightly *higher* frequency compared to the non-disordered case, despite the intuitive expectation that disorder should lead to a ‘softening’ of the spin waves. This upward shift is correspondingly manifest in an initial decrease in the uniform static susceptibility $\chi_u = N^{-1} \sum_{ij} \chi_{ij}^{-+}(0)$ upon the introduction of disorder: as follows from the Lehmann representation of the susceptibility Eq. (2.7), a decrease in density of low-frequency excitations with significant weight in the on-site spin flip subspace leads to a decrease in χ_u . On increasing disorder further, the UHF

single-particle gap closes and the pure Stoner spectrum acquires weight down to $\omega = 0$, Fig. 5. The maximum in the Stoner-like band in the RPA spectrum —occurring at $\omega \sim U$ — changes little with disorder, but its disorder-induced broadening increasingly repels the spin wave-like band which is thus by contrast shifted to *lower* frequency (see Fig. 5). This is the ‘softening’ of spin waves with disorder, which in turn is reflected in an increase in the uniform static susceptibility χ_u . Fig. 6 shows the disorder-averaged χ_u vs Δ/t for $U/t = 12$ (and we add that in the non-disordered limit, the resultant χ_u for the $N = 64$ site system reproduces accurately the $N \rightarrow \infty$ value, which can be obtained analytically). The above behaviour is clearly demonstrated: after an initial slight decrease, χ_u progressively increases with increasing disorder as the spin wave-like band moves to lower frequencies. Note further that increasing disorder for fixed U/t has a considerably less pronounced effect on the spin wave-like band than decreasing U/t for fixed disorder: decreasing interaction strength shifts the maximum in the Stoner-like band to lower energy (Fig. 4), while increasing Δ/t by contrast merely broadens the band, as shown in Fig. 5.

The effect of disorder on the position of the spin wave-like band also provides a natural explanation for the strongly site-differential enhancements of local susceptibilities with disorder, as found in a recent RPA study of the present model¹³. Specifically, the total uniform susceptibility is deconvoluted via

$$\chi_u = \int d\epsilon g(\epsilon) \chi(\epsilon) \quad (4.2)$$

where $\chi(\epsilon) = N_\epsilon^{-1} \sum_{i:\epsilon_i=\epsilon} \chi_i$ with $\chi_i = \sum_j \chi_{ij}(0)$. $\chi(\epsilon)$ is thus the mean local susceptibility for sites of *given* site energy ϵ . In ref. 13 (Fig. 2) it was found that an increase in disorder leads to a strong enhancement of $\chi(\epsilon)$ for sites in the local moment range $|\epsilon| \lesssim \frac{1}{2}U$, while sites outside this range, whose susceptibilities have typical Pauli-like values, are by contrast only weakly affected by disorder. A site-differential analysis of the RPA excitations forming the spin wave-like band, in analogy to $H(\epsilon; E)$ for single-particle states (Eq. (4.1)), shows that these excitations have weight almost exclusively on the strong local moment-carrying sites, and receive little contribution from sites outside the local moment range (consistent

with their interpretation as ‘spin wave’-like). As discussed above, the principal effect of increasing disorder is ultimately to shift the spin wave-like band to low frequency, while the Stoner-like band is merely broadened. The disorder-induced ‘softening’ of the spin wave-like band therefore manifests itself almost exclusively in $\chi(\epsilon)$ for strong moment-carrying sites, as found in Ref. 13; and has little effect on susceptibilities outside the local moment range, which are instead dominated by Stoner-like excitations.

C. Character of the transverse excitations

From the preceding section, it is clear (Figs 4,5) that a low-energy feature in the density of RPA transverse spin excitations indeed exists in the AF region of the $(\Delta/t, U/t)$ phase plane. However, the preceding analysis by itself gives no information on the spin wave-like *character* of the excitations which form this band, or with which sites they are associated. To probe the nature of these low-energy excitations, we have performed pole searches using $N = 216$ sites for many disorder realizations at a selection of points in the $(\Delta/t, U/t)$ plane, focusing (as in the non-disordered limit) on the lowest N excitations, with $\Omega(\omega_p) = 1/(U^2|\partial\lambda/\partial\omega|_{\omega=\omega_p})$ evaluated at each RPA pole. For illustration, the second and third columns respectively of Table I show $\Omega(\omega)$ averaged over the lowest N RPA excitations for (a) fixed $\Delta/t = 3$ and various interaction strengths U/t ; and (b) for fixed $U/t = 12$ as a function of disorder.

For fixed $U/t = 12$, it is seen that while increasing disorder leads to a diminution of spin wave character, the effect is relatively weak and the low energy transverse spin excitations retain strong spin wave character. This is consistent with the fact that the system remains an AF insulator, and with the persistence (Fig. 5) of the pronounced low energy spin wave-like band in the transverse spin spectrum. By contrast, reducing U/t at fixed disorder leads to a more pronounced reduction in spin wave character, consistent with the progressive erosion of the spin wave-like component in the RPA transverse spin spectrum (Fig. 4) discussed above. Again, this is physically natural: with decreasing interaction strength the system undergoes a (gapless) insulator→metal transition at $U/t \simeq 7.2$ and an increase in off-site

character in the low-energy spin excitations is thus to be expected. Note however that, even at low U/t , the RPA excitations have substantially more spin wave character than pure Stoner excitations in the same frequency range, as may be verified by considering the weight of the latter in the on-site spin flip subspace, given by

$$\Omega_{\text{HF}}(\omega_p^0) = \sum_{i\sigma} \sum_{\alpha>\beta} a_{i\alpha\sigma}^2 a_{i\beta-\sigma}^2 \delta(\omega_p^0 - [E_{\alpha\sigma} - E_{\beta-\sigma}]) \quad (4.3)$$

This is found to be an order of magnitude smaller than the corresponding $\Omega(\omega)$ for low-frequency RPA excitations.

D. Localization characteristics of low- ω excitations

Loss of translational symmetry on the introduction of disorder is expected to lead to localization of some or all collective excitations, in analogy to Anderson localization of single-particle states. Consider the IPR $L(\omega_p)$ of a collective transverse spin excitation of energy ω_p , as defined in Eq. (2.13). To distinguish between localized and delocalized excitations a threshold IPR appropriate to a given system size should be established, such that excitations below (above) this value are deemed extended (localized). In principle, this could be obtained by finite-size scaling, but in practice we are limited to system sizes on the order of $N = 216$. For single particle states of the non-interacting Anderson model, finite-size scaling yields a threshold IPR $L'_c \sim 0.1$ for $N = 216$ sites. We correspondingly adopt a threshold $L_c \sim 0.1$ for collective excitations of the Anderson-Hubbard model. This value itself should not of course be taken very seriously; it simply serves as a useful qualitative guide in the following discussion.

Fig. 7 shows the IPR $L(\omega)$ of the lowest energy excitations for $U/t = 12$ and various values of the disorder. For weak $\Delta/t = 1.5$ (Fig. 7 A), the majority of excitations are delocalized, as expected, with a localized ‘tail’ at high ω . Increasing disorder to $\Delta/t = 3$ and 4.5 leads to the occurrence of further sparse, localized excitations at very low ω , superimposed over a background of delocalized excitations (Fig. 7 B,C); and the density of localized excitations rises on further increasing disorder (Fig. 7 D).

The above behaviour is clarified by considering the corresponding IPR probability distributions, $P(L)$ (Fig. 8). This shows a peak at low L , corresponding to the ‘delocalized’ backbone, with a long tail to high L , reflecting the presence of localized excitations. For low $\Delta/t = 1.5$, the peak is sharp and centred well within our approximate criterion for delocalized excitations. As Δ/t is increased, the distribution broadens and the most probable value of L shifts to higher values.

To understand the above behaviour, we site-resolve excitations of given IPR L , in analogy to the site distribution of quasiparticle states, $H(\epsilon; E)$ (Eq. (4.1)), via the quantity

$$H_{\text{RPA}}(\epsilon; L) = \frac{g(\epsilon)N_{\text{RPA}}(\epsilon; L)}{N_{\text{RPA}}(L)} \quad (4.4)$$

(such that $\int d\epsilon H_{\text{RPA}}(\epsilon; L) = 1$). Here, $N_{\text{RPA}}(L) = N^{-1} \sum_{\omega_p} \delta(L - L(\omega_p))$ is the density of excitations of fixed IPR L , and $N_{\text{RPA}}(\epsilon; L)$ is the partial density of such excitations on sites of given site energy ϵ , given by

$$N_{\text{RPA}}(\epsilon; L) = N_{\epsilon}^{-1} \sum_{i: \epsilon_i = \epsilon} \sum_{\omega_p} |V_{i\gamma}(\omega_p)|^2 \delta(L - L(\omega_p)). \quad (4.5)$$

$H_{\text{RPA}}(\epsilon; L)$ then gives the overlap of excitations of given IPR L on sites of different site energies. For $(\Delta/t, U/t) = (3, 12)$, Fig. 9 shows the ϵ -dependence of H_{RPA} averaged over all $L < 0.1$ and $L > 0.3$, to illustrate the site-differential character of extended and localized excitations respectively. Localized excitations are seen to be dominated by sites close to the local moment boundaries $|\epsilon| \sim U/2$, while sites in the range $|\epsilon| \lesssim U/2$, which carry large moments, make the dominant contribution to delocalized excitations. As expected, sites outside the local moment regime, which possess very small moments, do not contribute significantly to any of the low energy excitations; rather, they participate in Stoner-like excitations of significantly higher energy.

The origin of the localized and delocalized low energy transverse spin excitations is then readily rationalized. Sites with site energies in the range $|\epsilon| \lesssim U/2$, which possess large local moments, contribute most significantly to single particle states within the Hubbard subbands. Since these states are the most delocalized, collective excitations involving them will

likewise be delocalized. At UHF (‘pure Stoner’) level, transverse spin excitations between single-particle states within the Hubbard bands incur an energy cost of order U ; but in the RPA spectrum, via inclusion of particle-hole correlations, this energy is renormalized down to a spin wave-like scale on the order of an exchange coupling. This is the origin of the delocalized low-energy transverse spin excitations. By contrast, sites with $|\epsilon| \sim U/2$ close to the local moment boundaries participate dominantly in single-particle states close to the Fermi level, or an energy $\sim U$ above or below it. For $U/t = 12$ such states are strongly localized, hence so too are collective excitations involving them. Again, such excitations are renormalized to a low-energy scale via the particle-hole interactions inherent in the RPA. Both localized and delocalized transverse spin excitations thus arise at low energies, reflecting the underlying localization characteristics of single particle states over a very wide energy range in the associated single-particle spectrum. Note further that these arguments do not imply coexistence of localized and extended transverse spin excitations at the same energy in the spin wave-like band; and the apparent occurrence of such in eg Fig. 7D is largely a consequence of sampling different disorder realizations. While the present, qualitative considerations do not of course permit identification of mobility edges in the spin wave-like band, it is at least plausible from Fig. 7 that such exist.

From the above, the system can thus be regarded as composed of two essential components: an AF large-moment component which gives rise to the backbone of delocalized excitations, and a set of sites carrying smaller moments which give rise to localized excitations. As disorder is increased, the fraction of sites in the former category decreases, leading to a shift in the peak in $P(L)$ (Fig. 8) to higher L and a concomitant broadening of the distribution. The probability of sites with $|\epsilon| \sim U/2$ correspondingly increases, and hence localized excitations ultimately become the dominant theme.

The above discussion is confined to a region of the $(\Delta/t, U/t)$ phase diagram in which the mean field ground state is an AF insulator. What of the metallic AF and SG phases? Fixing $\Delta/t = 3$ and decreasing U/t progressively from $U/t = 12$ down to $U/t = 6$ leads (at $U/t \simeq 7.2$) to a transition from an AF insulator to an AF metal. However, the IPR

profile of the low-energy transverse spin excitations shows essentially no qualitative change from that for $U/t = 12$: a backbone of delocalized excitations remains present, with localized excitations superimposed at low and higher ω/t . In the metallic region, however, the localized excitations now arise principally from transfer of a spin between a *delocalized* UHF state near the Fermi level to a *localized* UHF state $\sim U$ above or below E_F . The localized state overlaps only a few sites, while the delocalized state has weight on a finite fraction of sites. The excitation thus appears localized in the IPR profile since the on-site spin flip contribution (which is of course the component of the excitation probed, see Eq. (2.14)) can occur only from sites overlapped by the localized state.

On decreasing U/t further to $U/t \simeq 2.5$, the mean field ground state becomes a SG metal. Here, the RPA and pure Stoner excitation spectra appear virtually identical (see e.g. Fig. 4). It is indeed found that the majority of low energy RPA excitations are little more than weakly renormalized Stoner excitations, as expected from the low value of $\bar{\Omega}$ in Table I. However, at very low energies ($\omega \lesssim 0.3t$), this is not the case. As in the AF metal regime, low energy localized modes appear in the RPA spectrum, while the pure Stoner spectrum at such low energies is composed of entirely delocalized modes (since the system is metallic). These localized excitations are found to have dominant weight on those rare sites in the spin glass that possess substantial local moments, flips of which would incur an energy cost of $\sim U$ within UHF, but occur at significantly lower energies in the RPA spectrum.

V. DISCUSSION

In recent papers^{14,15}, we have described an approximate mapping of the low-frequency transverse spin excitations of the non-disordered Hubbard model at finite U/t , on to those of an effective underlying Heisenberg model. The U/t -dependent effective exchange couplings are not restricted to purely nearest neighbour interactions; they follow solely from a knowledge of the RPA excitations about the broken-symmetry UHF state at zero temperature. The mapping becomes exact as $U/t \rightarrow \infty$ and, conjoined with an Onsager reaction

field approach, enables extraction of thermodynamic properties in the thermal paramagnetic phase. The resultant Néel temperatures, spin correlation functions and magnetic susceptibilities were^{14,15} found to be in good agreement with Quantum Monte Carlo calculations over a wide U/t -range from strong to weak coupling. We now assess the extent to which the present findings support application of such a mapping to the Anderson-Hubbard model.

As discussed in Refs 14, 15, the mapping is accurate provided there is a persistent separation between low energy spin wave-like excitations and higher energy Stoner-like excitations; i.e. provided in practice a discernible spin wave-like band, comprising excitations with an appreciable degree of on-site spin flip character, is present in the full RPA transverse spin spectrum. As shown in §III, this indeed holds for the pure Hubbard model for all $U/t \gtrsim 2-3$. For the Anderson-Hubbard model, Fig. 5 and Table I show that this also holds for all disorder strengths studied, at relatively large $U/t = 12$. Thus, the mapping should certainly be accurate well within the disordered AF phase of the model. On fixing disorder and reducing interaction strength towards the AF-SG boundary, the spin wave character of the low-frequency band decreases significantly and the band itself is ultimately absorbed by the Stoner-like portion, such that for $\Delta/t = 3$ the mapping would not be quantitatively accurate for $U/t \simeq 4$ and below. Not unexpectedly, therefore, the mapping would not be applicable to the low- U/t SG phase; but we do anticipate it to be accurate throughout the major part of the disordered AF phase in the $(\Delta/t, U/t)$ plane, wherein the effect of disorder on, for example, the Néel temperature can be investigated. This is the subject of a forthcoming paper²⁰.

ACKNOWLEDGMENTS

We are grateful to the EPSRC (Condensed Matter Physics) for financial support.

REFERENCES

- ¹ T. Kennedy, E. H. Lieb and B. S. Shastry, J. Stat. Phys. **53**, 1019 (1988).
- ² P. W. Anderson, Phys. Rev. **86**, 694 (1952); T. Oguchi, Phys. Rev. **117**, 117 (1960).
- ³ E. Manousakis, Rev. Mod. Phys. **63**, 1 (1991).
- ⁴ Y. L. Wang, S. Shtrikman and H. Callen, Phys. Rev. **148**, 419 (1966).
- ⁵ P. W. Anderson, *Concepts in Solids* (Benjamin, Reading, MA, 1963).
- ⁶ K. Yonemitsu, I. Batistić, and A.R. Bishop, Phys. Rev. B **44**, 2652 (1991).
- ⁷ A. Singh and Z. Tesanović, Phys. Rev. B **41**, 614 (1990); *ibid* **41**, 11457.
- ⁸ J. R. Schrieffer, Z.-G. Wen and S.-C. Zhang, Phys. Rev. B **39**, 11663 (1989).
- ⁹ P. Sen and A. Singh, Phys. Rev. B **48**, 15792 (1993).
- ¹⁰ D. R. Penn, Phys. Rev. **142**, 350 (1966).
- ¹¹ M. A. Tusch and D. E. Logan, Phys. Rev. B **48**, 14843 (1993).
- ¹² D. G. Rowan, Y. H. Szczech, M. A. Tusch and D. E. Logan, J. Phys.: Condensed Matter **7**, 6853 (1995).
- ¹³ M. A. Tusch and D. E. Logan, Phys. Rev. B **51**, 11940 (1995).
- ¹⁴ M. A. Tusch, Y. H. Szczech and D. E. Logan, Phys. Rev. B **53**, 5505 (1996).
- ¹⁵ Y. H. Szczech, M. A. Tusch and D.E. Logan, Phys. Rev. Lett. **74**, 2804 (1995).
- ¹⁶ A. L. Fetter and J. D. Walecka, *Quantum Theory of Many-Particle Systems* (McGraw-Hill, New York, 1971).
- ¹⁷ D. J. Thouless, *The Quantum Mechanics of Many-Body Systems* (Academic, New York, 1972).
- ¹⁸ R. J. Bell and P. Dean, Disc. Faraday Soc. **50**, 55 (1970).

¹⁹ T. M. Chang, J. D. Bauer and J. L. Skinner, J. Chem. Phys. **93**, 8973 (1990).

²⁰ Y. H. Szczech, M. A. Tusch and D. E. Logan, J. Phys.: Condensed Matter **10**, 639 (1998).

FIGURES

FIG. 1. Density of low-frequency RPA excitations $N_T(\omega)$ for the pure Hubbard model with $U/t = 20$ (solid line), compared to the linear spin wave spectrum of the pure AF Heisenberg model with nearest-neighbour $J = 4t^2/U$ (dashed line).

FIG. 2. Density of the N lowest-frequency RPA excitations $N_T(\omega)$ for the pure Hubbard model for increasing interaction strengths: $U/t = 2$ (a), 3 (b), 4 (c), 6 (d), 8 (e), 12 (f), 20 (g).

FIG. 3. For $U/t = 12$ and $\Delta/t = 3$, (A) Disorder-averaged density of UHF single-particle states $D(E)$ vs E/t (solid line), where the unperturbed ($U = 0$) bandwidth is $12t$; IPR $L'(E)$ for $N = 512$ site systems (dashed line); (B) Corresponding site-resolved local moment distribution $|\mu(\epsilon)|$ vs site energy ϵ/t (solid line, left-hand scale), $H(\epsilon; E_F)$ as defined in text (dashed line, right-hand scale).

FIG. 4. Full transverse excitation spectrum for the Anderson-Hubbard model at RPA level (solid line) for $N = 64$ averaged over many disorder realizations, compared to the corresponding UHF Stoner spectrum (dashed) for fixed disorder $\Delta/t = 3$ and $U/t = 12$ (a), 9 (b), 6 (c), 3 (d)

FIG. 5. As Fig. 4 but with fixed interaction strength $U/t = 12$ and $\Delta/t = 1$ (a), 2 (b), 3 (c), 4.5 (d), 6 (e) and 7.5 (f). Note the persistence of a spin wave-like band for all disorder strengths.

FIG. 6. Uniform RPA static transverse susceptibility χ_u for fixed $U/t = 12$ as a function of disorder Δ/t .

FIG. 7. Scatter diagram showing IPR L for low-frequency RPA excitations vs ω/t for fixed interaction strength $U/t = 12.0$ and varying disorder, $\Delta/t = 1.5$ (A), 3.0 (B), 4.5 (C), 6.0 (D).

FIG. 8. Probability distribution of IPRs $P(L)$ for $U/t = 12$ and $\Delta/t = 1.5$ (solid), 3.0 (dashed), 4.5 (dot-dashed) and 6.0 (dotted).

FIG. 9. Probability distribution $H_{\text{RPA}}(\epsilon; L)$ (Eq. (4.4)) of the lowest N RPA excitations with IPR L over sites of energy ϵ , averaged over excitations with $L > 0.3$ (solid line) and $L < 0.3$ (dotted line) for $U/t = 12$ and $\Delta/t = 3$.

TABLES

TABLE I. Spin wave character of low- ω RPA excitations Ω for the non-disordered and disordered Hubbard models. For $\Delta/t = 0$, $\Omega = \Omega(\omega_{\max})$; $\bar{\Omega}$ is the average of $\Omega(\omega)$ over the lowest N excitations.

$\Delta/t = 0$		$\Delta/t = 3.0$		$U/t = 12$	
U/t	Ω	U/t	$\bar{\Omega}$	Δ/t	$\bar{\Omega}$
1.0	0.02	3.0	0.05	0.0	1.00
2.0	0.39	4.5	0.20	1.5	1.00
3.0	0.71	6.0	0.33	3.0	0.98
4.0	0.86	9.0	0.75	4.5	0.89
≥ 5.0	1.00	12.0	0.98	6.0	0.88

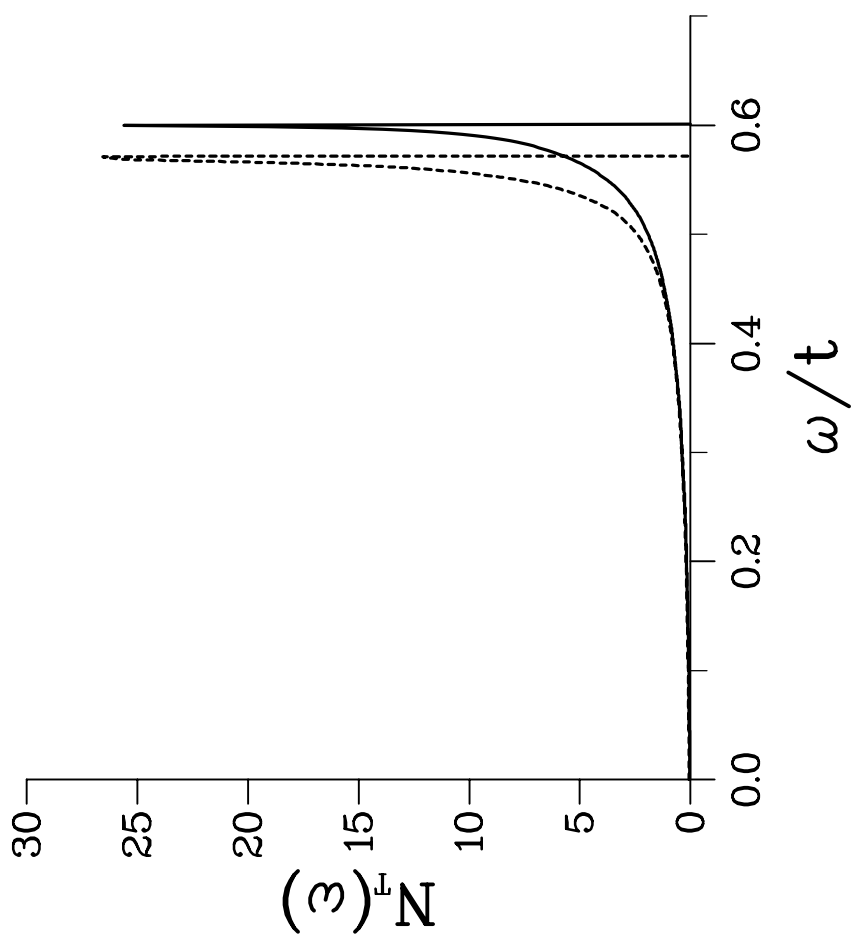


FIG. 1

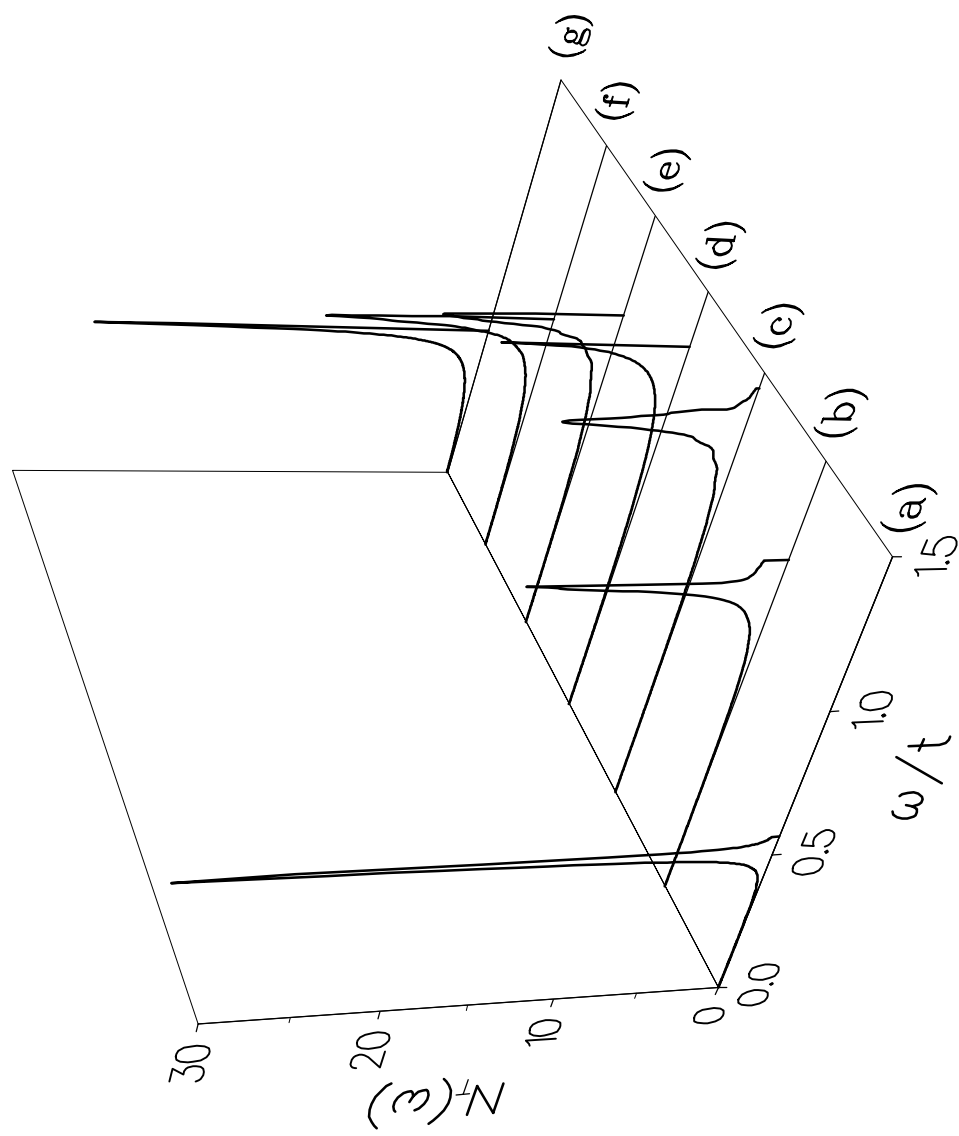


FIG. 2

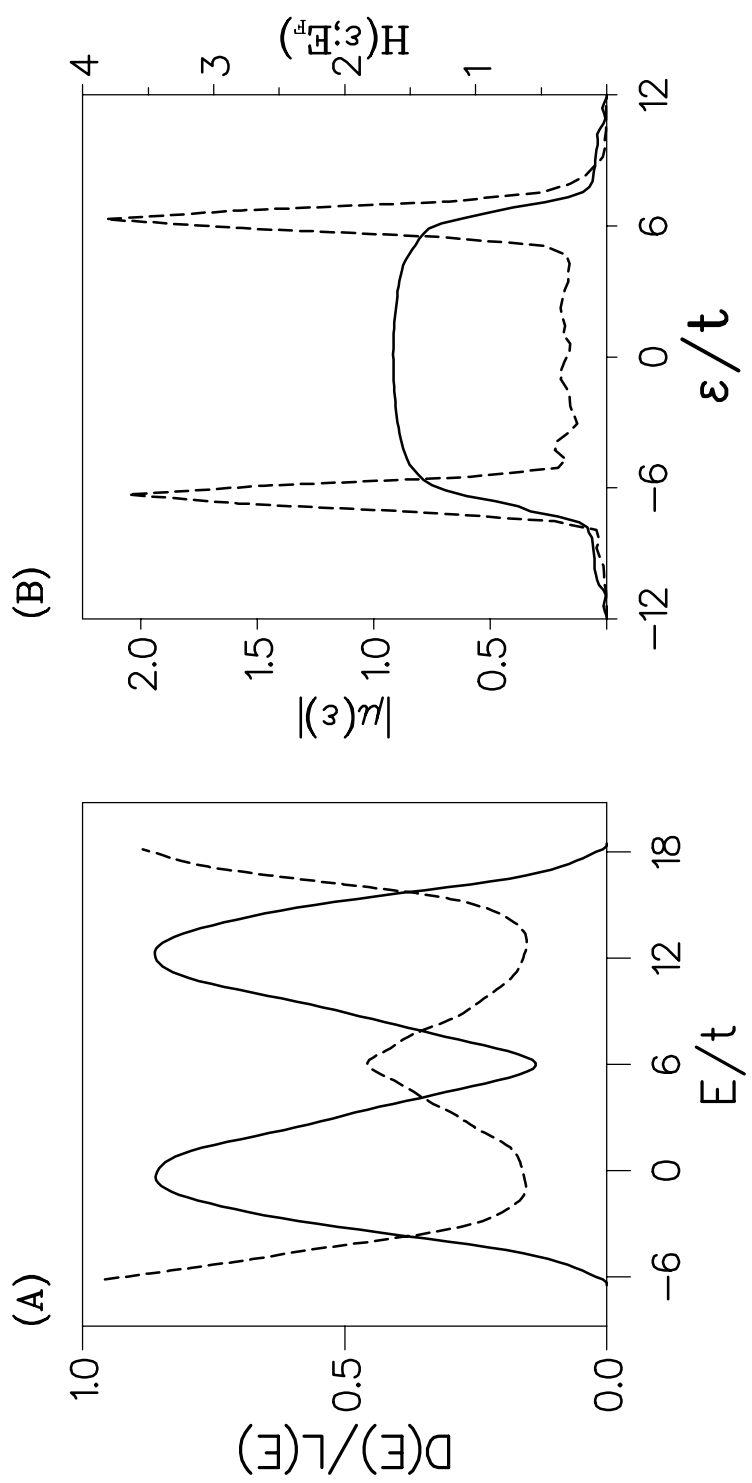


FIG. 3

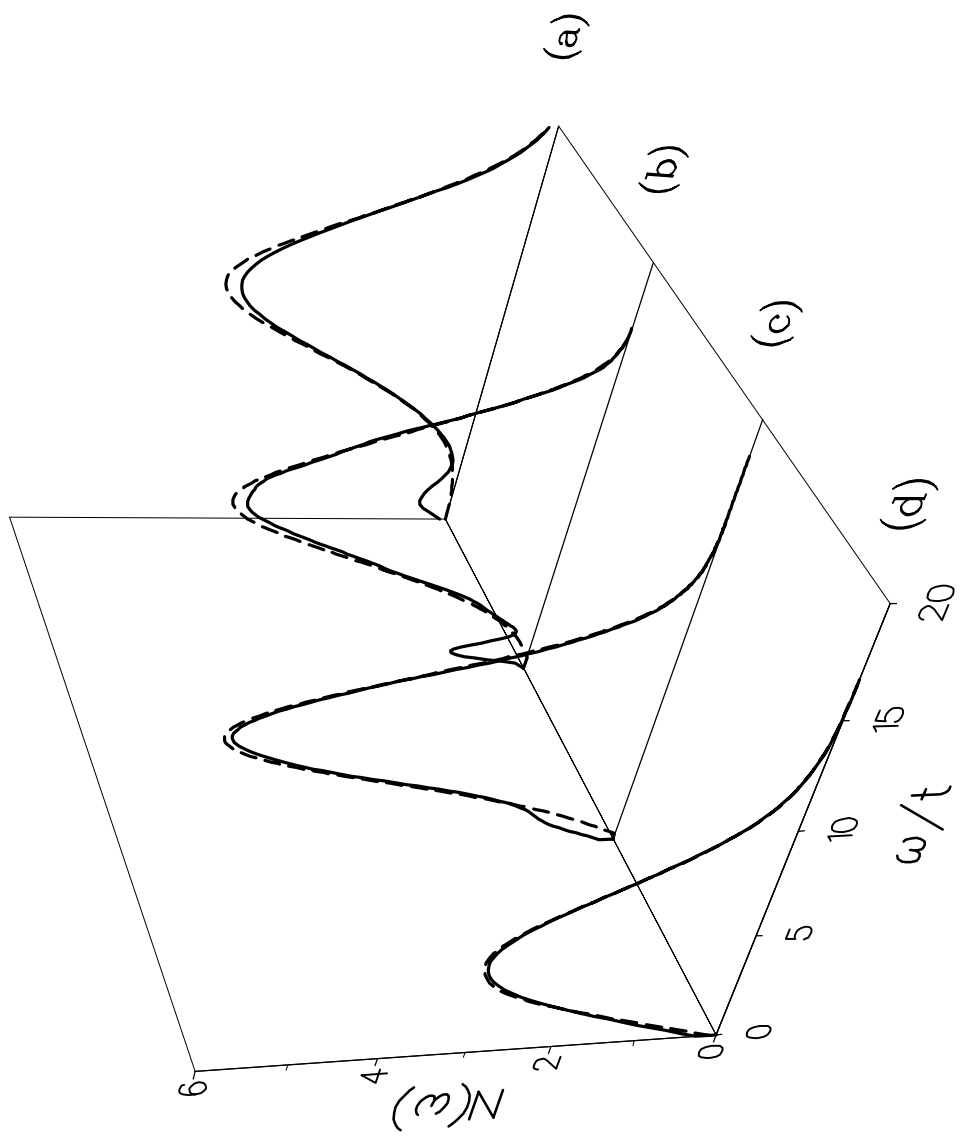


FIG. 4

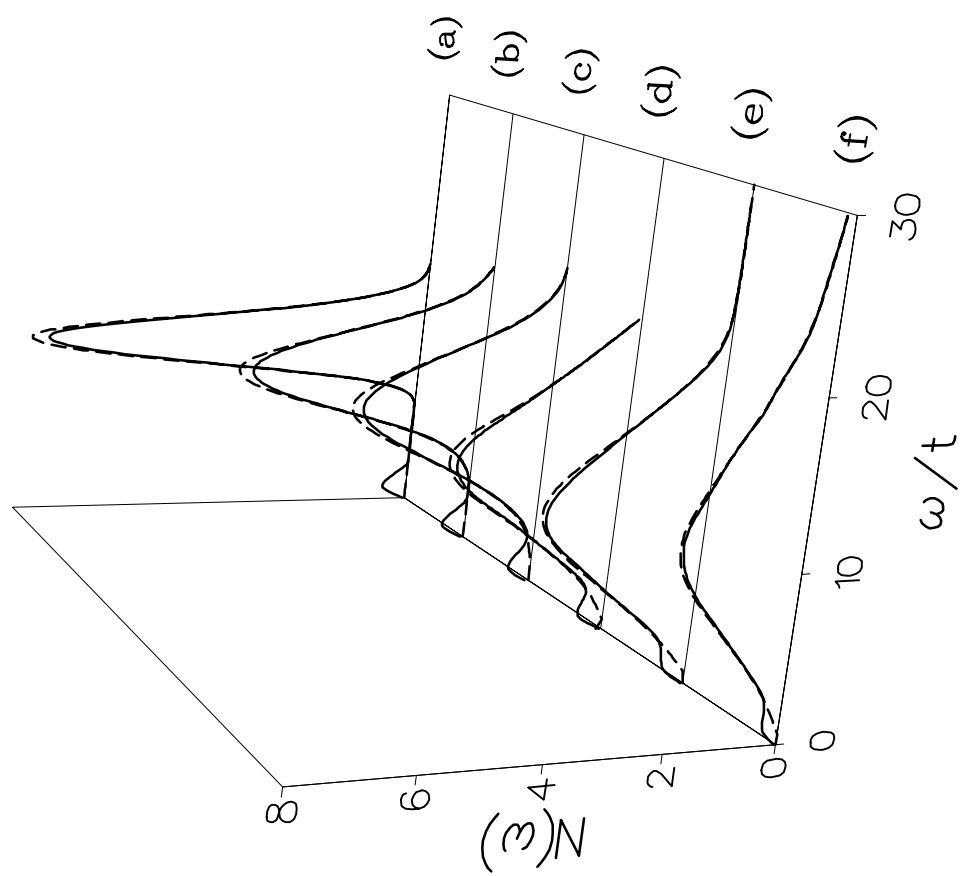


FIG. 5

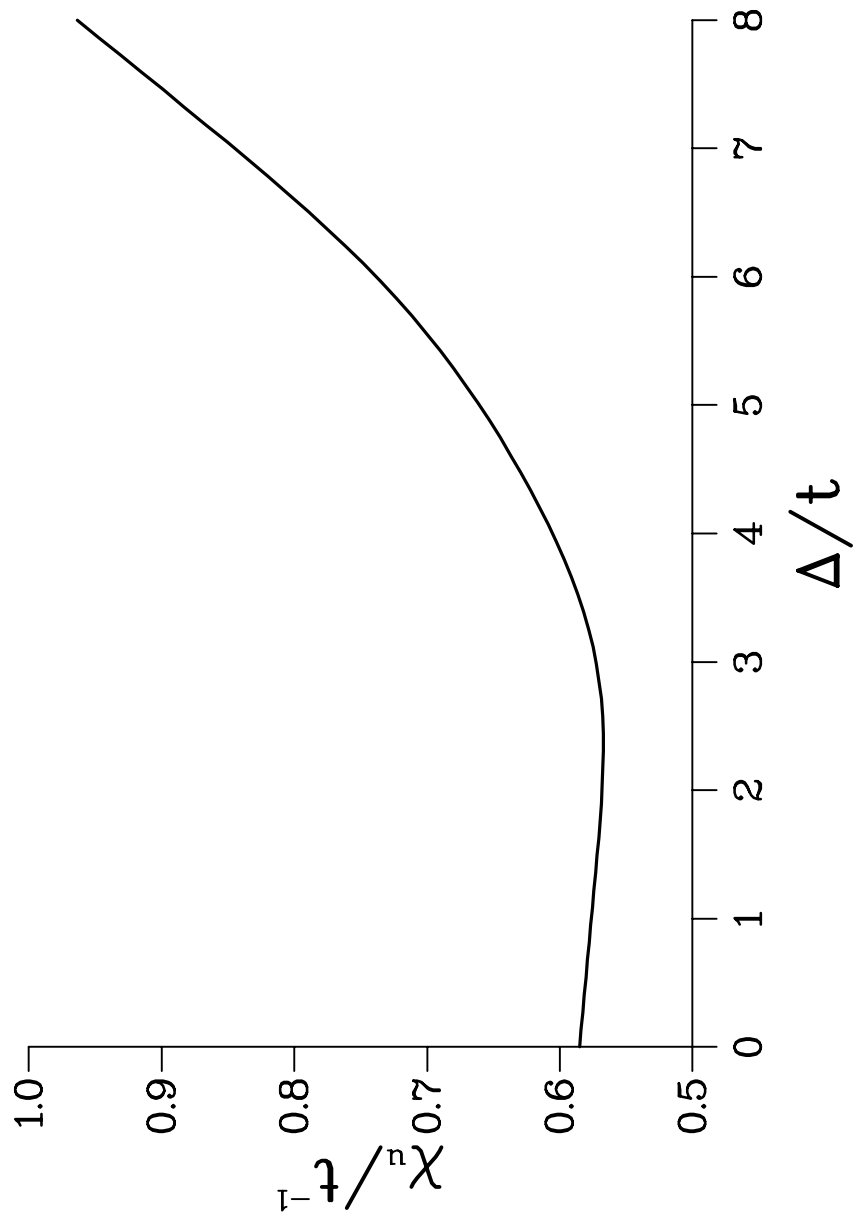


FIG. 6

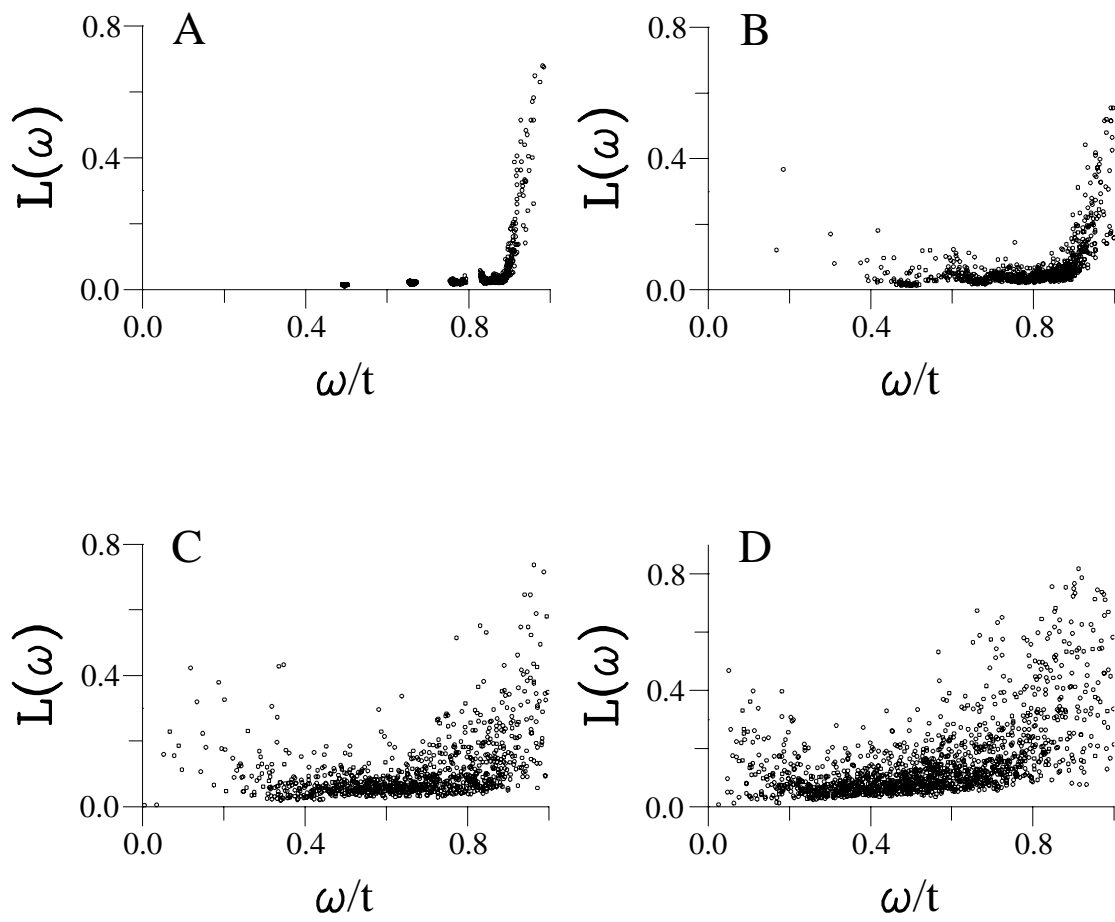


FIG. 7

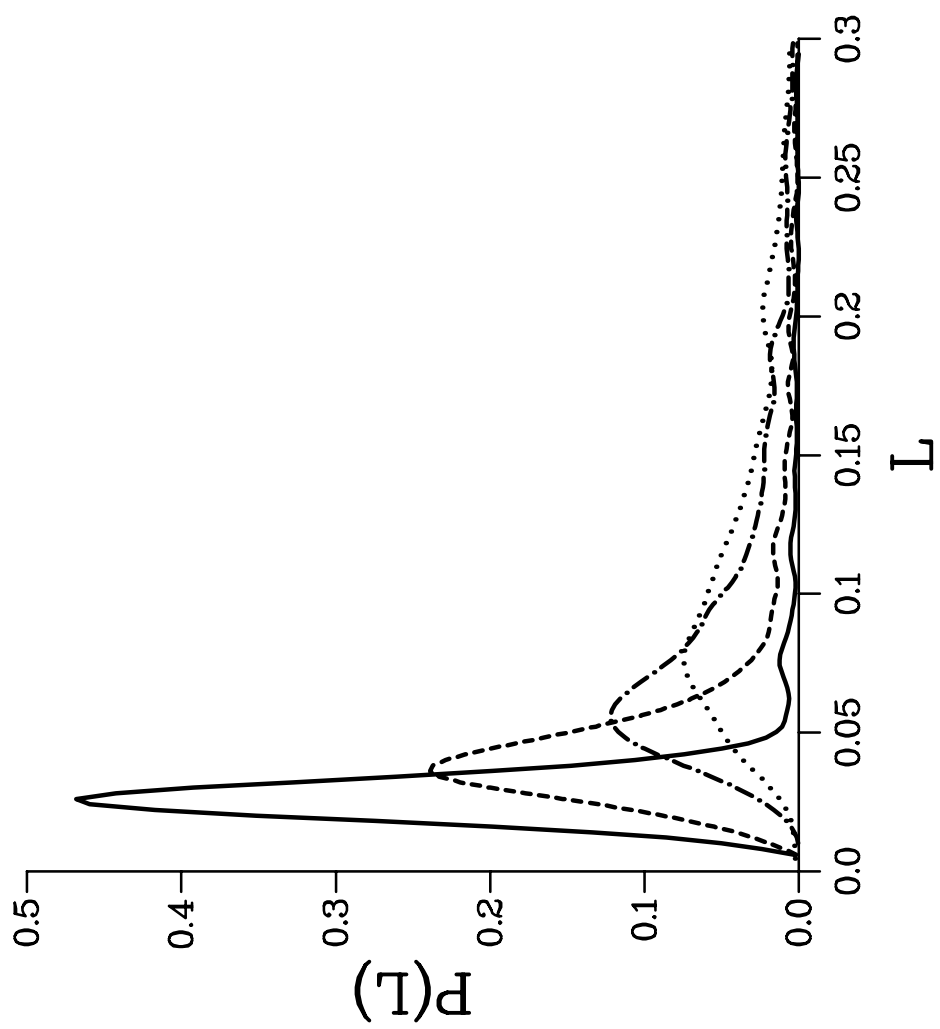


FIG. 8

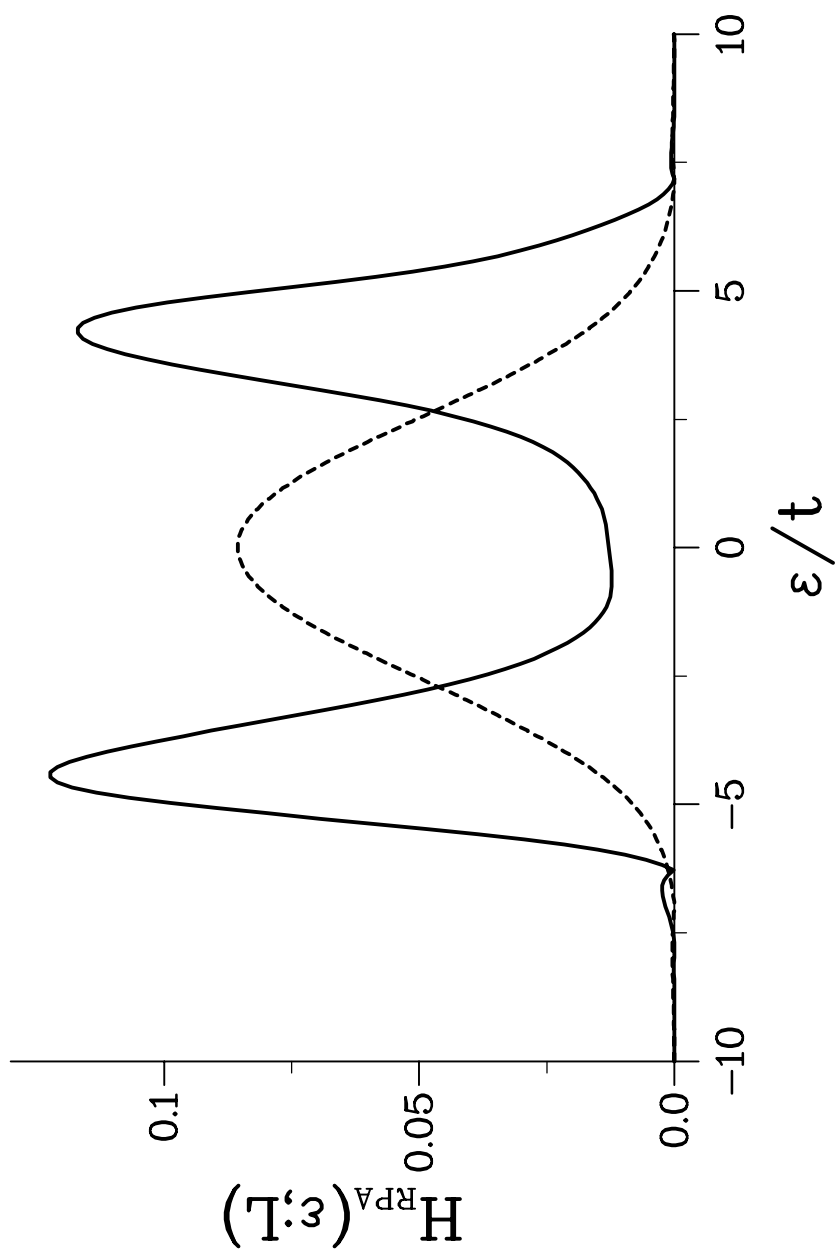


FIG. 9